

Hydrogen-induced volume changes, dipole tensor, and elastic hydrogen-hydrogen interaction in a metallic glass

Johan Bylin ¹, Paulius Malinovskis ¹, Anton Devishvili ², Ralph H. Scheicher ³, and Gunnar K. Pálsson ^{1,*}

¹*Division of Materials Physics, Department of Physics and Astronomy, Uppsala University, Box 516, SE-75121 Uppsala, Sweden*

²*Institut Laue-Langevin, 71 avenue des Martyrs, 38000 Grenoble, France*

³*Division of Materials Theory, Department of Physics and Astronomy, Uppsala University, Box 516, SE-75121 Uppsala, Sweden*



(Received 27 April 2022; revised 7 September 2022; accepted 9 September 2022; published 29 September 2022)

Hydrogen and its isotopes, absorbed in metals, induce local stress on the atomic structure, which generates a global expansion in proportion to the concentration of hydrogen. The dipole force tensor and its interaction with the stress fields give rise to an effective attractive nonlocal potential between hydrogen atoms—the elastic hydrogen-hydrogen interaction—which is a key quantity governing the phase transitions of hydrogen in metals. While the dipole tensor and the elastic interaction have been researched in crystalline materials, they remain experimentally unexplored in metallic glasses and it is unclear how these quantities are affected by the lack of point group symmetries. Here, we investigate both experimentally and theoretically the volume changes, the components of the force dipole tensor, and ultimately the elastic hydrogen-hydrogen interaction in the metallic glass $V_{80}Zr_{20}$. *In situ* neutron reflectometry was used to determine the deuterium-induced volume changes as a function of deuterium concentration. The one-dimensional volume expansion is found to change by more than 14% without any structural degradation, up to concentrations of one deuterium atom per metal atom. From the expansion, we determine that the out-of-plane component of the elastic dipole tensor is remarkably similar to a composition weighted sum of the ones found in crystalline vanadium and zirconium. Via *ab initio* calculations of both free and biaxially constrained expanded metallic structures, we determine that the trace of the dipole tensor varies with hydrogen concentration and is essentially invariant of global elastic boundary conditions. As a consequence, the elastic hydrogen-hydrogen interaction energy is found to be concentration-dependent as well, illustrating that the disordered nature of a metallic glass does not impede the mediation of the elastic attraction, but rather allows it to vary with hydrogen content.

DOI: [10.1103/PhysRevB.106.104110](https://doi.org/10.1103/PhysRevB.106.104110)

I. INTRODUCTION

Hydrogen and its isotopes can be absorbed in large quantities in many crystalline and amorphous metals. Such materials have, for example, been considered for energy storage [1], hydrogen sensing [2], hydrogen purification [3], and metal hydride batteries [4].

The volume changes caused by hydrogen are of crucial importance for understanding the cause of embrittlement in metals, which leads for instance to degradation in the performance of metal hydrides for energy storage [5]. The hydrogen-induced volume changes also carry valuable information about the local and global strain fields, which are responsible for the hydrogen-hydrogen (H-H) interaction and the condensation of the lattice-liquid and lattice-solid phases of hydrogen in materials [6–8]. The hydrogen-induced strain

fields can be captured conceptually via the dipole force tensor concept [9],

$$P_{ij} = \sum_m f_i^m r_j^m = \frac{\Omega}{c} \langle \sigma_{ij} \rangle, \quad (1)$$

where f_i^m is the force vector component exerted by a hydrogen atom on a metal atom m , located r_j^m from the hydrogen. With a homogeneous distribution of hydrogen atoms, constituting the atomic ratio c of hydrogen atoms per metal atom [H/M] in a metal of atomic volume Ω , it is possible to relate the average global stress $\langle \sigma_{ij} \rangle$ to the dipole tensor directly. Hence the dipole force tensor can be considered the connecting quantity between the local microscopic strain and the global elastic response.

When studying the volume expansion in crystalline metal hydrides, Peisl [10] found that hydrogen in many metals appear to occupy, on average, a volume of about 2.9 \AA^3 . In the same year, Switendick [11,12] predicted a minimum H-H distance of 2.1 \AA when calculating the band structures of metal hydrides, a distance which later became known as the Switendick criterion. Westlake [13,14] implemented this lower bound to construct a geometrical model with which he could predict the stoichiometry, stability, and hydrogen occupancy in metal hydrides. It was shown that the model was

*Corresponding author: gunnar.palsson@physics.uu.se

Published by the American Physical Society under the terms of the [Creative Commons Attribution 4.0 International license](https://creativecommons.org/licenses/by/4.0/). Further distribution of this work must maintain attribution to the author(s) and the published article's title, journal citation, and DOI. Funded by [Bibsam](https://www.bibsam.org/).

also consistent with Peisl's observation, as when Westlake examined hydrogen in intermetallic transition metal compounds, he found hydrogen volumes in an interval of 2.1 \AA^3 to 3.2 \AA^3 .

However, considering the distribution of local atomic environments of metallic glasses, two questions naturally arise: can hydrogen in metallic glasses also fulfill these empirical criteria and can the exerted dipole forces in these disordered materials create the conditions for the mediation of the nonlocal H-H interaction? Hence, to test the validity of the empirical criteria of hydrogen volumes as well as the theoretical understanding about the nature of hydrogen in amorphous metals, the global volume expansion, the dipole force tensor, and the elastic H-H interaction need to be determined, which is the main purpose of the present article.

The volume expansion has previously been measured in metallic glasses, mostly by observing the shift in the first amorphous peak in the x-ray diffraction pattern [15,16]. The analysis associated with determining the expansion from diffraction measurements is quite cumbersome and requires detailed knowledge of the composition and the pair distribution function. In the case of thin films, however, neutron reflectometry can be used to simultaneously determine the changes in the thickness and the absolute hydrogen concentration from fitting the reflectivity pattern to a film/substrate slab model with the additional benefit of not requiring information about the microscopic structure.

We have used the vanadium-rich $V_{80}Zr_{20}$ thin film metallic glass as a model system for this study, not only due to its practical use [17–21], but also from a fundamental perspective, because it contains the minimum number of elements to render it amorphous and stable in an extended range of temperatures. Another reason is to be able to compare the measured volume expansion to those found in crystalline vanadium and zirconium. For reasons having to do with the sensitivity of neutron reflectivity to hydrogen and its isotopes, we have chosen to measure the volume expansion exclusively with deuterium. However, the volume changes observed in bulk metals are essentially isotope independent [14]. We will therefore mention both isotopes interchangeably throughout the article.

To achieve greater insight into the nature of hydrogen in metallic glasses, we have also determined the hydrogen-induced volume changes, the dipole force tensor, and the H-H interaction energy via first-principles calculations in combination with the stochastic quenching (SQ) method [22].

II. EXPERIMENTAL AND THEORETICAL DETAILS

The films were grown by dc magnetron sputtering onto a $20 \text{ mm} \times 20 \text{ mm}$ amorphous SiO_2 substrate in an ultrahigh-vacuum chamber with a base pressure less than 3×10^{-10} Torr. To minimize the level of contaminants, argon of 6N purity was sent through a Nupure Omni 40 PF purifying filter in between the bottle and the sputter chamber. The substrate was annealed at 573 K for 30 min in ultrahigh vacuum to reduce the amount of water and other impurities on the surface and was subsequently cooled to room temperature before vanadium and zirconium were cosputtered. To protect the sample from oxidation and to facilitate the dissociation of deuterium, a 6 nm palladium capping layer was deposited on

top of the film. To minimize alloying of the palladium with the underlying film, temperatures were restricted to below 323 K during deposition and 448 K during the *in situ* measurements, which is well below the approximate 730 K crystallization temperature of amorphous $V_{80}Zr_{20}$ [23]. Rutherford backscattering spectrometry was used to verify the composition to within 1 at. % of the intended composition.

The equilibrium deuterium concentration in palladium is negligible in the measured temperature and pressure ranges as the enthalpy and entropy of hydrogen absorption in palladium only allows for at most 0.03 H/M [24]. This was also verified during the fitting of the neutron reflectivity.

The neutron data was gathered at the SuperAdam reflectometer [25] at the Institut Laue Langevin, Grenoble, France. The wavelength was $\lambda = 5.21 \text{ \AA}$ and the resolution was determined to be $\Delta Q = 0.007 \text{ \AA}^{-1}$ with a beam size of 1.5 mm in the scattering plane and 30 mm out of the scattering plane. The measured reflected angle θ was transformed to a scattering wave vector via $Q = 4\pi \sin(\theta)/\lambda$. The sample was measured in a specially designed ultrahigh vacuum neutron scattering chamber, capable of gas loading a wide range of deuterium pressures. The chamber was baked out together with the sample for 36 h at 423 K prior to the experiment. The pressure was dosed from a pressurized deuterium bottle of 5N purity (isotopic purity 2N). The deuterium gas was subsequently let through a Nupure UltraPure 40 purifier to ensure less than 1 ppb of contaminants in the gas. The entire chamber was heated from the outside using a Hemi heating jacket to minimize thermal gradients. The temperature was regulated using a Lakeshore 334 temperature controller to within 0.1 K, using a type-K thermocouple in mechanical contact to the backside of the substrate.

The sample was exposed to a series of stepwise increasing deuterium gas pressures, continuously maintained at a fixed temperature. At each pressure plateau, a neutron reflectivity curve was measured. After reaching a pressure of about 500 mbar, the chamber was evacuated and the film was allowed to spontaneously desorb before another temperature was chosen. In total three temperatures were chosen to examine whether the expansion in thin film metallic glasses is temperature dependent.

The raw neutron reflectivity patterns were corrected for overillumination, divided by the monitor count rate and the direct beam intensity, and a background, taken from either side of the specular ridge, was subtracted using the in-house software for SUPERADAM [25].

The reflectivity patterns were fitted using a slab model as implemented in the GENX program [26,27], which includes resolution, roughness, and multiple scattering effects. From the fit, the scattering length density ρ_s was determined, given by

$$\rho_s = \frac{\rho N_A \sum_i c_i b_i}{\sum_i c_i M_i}, \quad (2)$$

where ρ is the mass density of the material, N_A is Avogadro's number, c_i is the atomic concentration of species i (V, Zr, or D), M_i are the corresponding atomic weights, and b_i are the bound coherent scattering lengths of element i (here, the relevant scattering lengths are $b_V = -0.3824 \text{ fm}$, $b_{Zr} = 7.161$

fm, and $b_D = 6.671$ fm [28]). If the composition and density of the material is known without deuterium, the concentration can thus be extracted via Eq. (2) using the fitted scattering length density. The fitting parameters of the slab model were fixed by the reference reflectivity pattern corresponding to an unloaded sample and, for all succeeding measurements, only the thickness and scattering length density of the $V_{80}Zr_{20}$ layer was allowed to change; all other parameters were kept constant.

For the first-principles calculations, density functional theory [29,30] as implemented in the Vienna Ab initio Simulation Package (VASP) [31–33], along with the generalized gradient approximation (GGA) correlation functional of Perdew, Burke, and Ernzerhof (PBE) [34] was used to construct amorphous candidate structures via the stochastic quenching procedure [22]. This method generates amorphous structures in the sense that the position of all atoms are initially random, with a minimum separation of one atomic radius, but are subsequently allowed to relax until the Feynman-Hellman forces acting on the atoms are zero within a threshold of 20 meV/Å. A cubic supercell of size $14 \text{ Å} \times 14 \text{ Å} \times 14 \text{ Å}$ with 140 vanadium atoms and 35 zirconium atoms was constructed in order to fulfill the system size criteria proposed by Holmström and co-workers [22]. We examined the system size convergence by constructing a reference $12 \text{ Å} \times 12 \text{ Å} \times 12 \text{ Å}$ sized system. The associated volume expansion coefficient for concentrations of $c = 0.2, 0.4, 0.6, 0.8$ H/M was found to be the same as the one for the $14 \text{ Å} \times 14 \text{ Å} \times 14 \text{ Å}$ system within 0.4%, demonstrating the validity of the random valley approximation. For this reason, and to make the isotropic and clamped expansion as comparable as possible, we worked exclusively with the $14 \text{ Å} \times 14 \text{ Å} \times 14 \text{ Å}$ system. Each calculation was performed with an energy cutoff of 450 eV, a k -point sampling including only the Γ point, and the Methfessel-Paxton method [35] using 0.2 eV as smearing width. The energy convergence criteria was set to 10^{-6} eV. Once an amorphous configuration was created, the elastic constants were determined by applying a series of strains to each of the principal axes and the components of the stress tensor were calculated in each case. The stress vs strain curves were then fitted to a first-order polynomial and the elastic constants were extracted. We averaged the constants over the three directions to arrive at values that are representative for the isotropic solid.

Hydrogen at selected concentrations was added to the amorphous candidate configuration, using an algorithm that inserted the hydrogen at random, subject to the constraint that it would be sufficiently separated to any other atom, which, as a starting point, was larger than the Switendick criterion. This distance criterion was systematically varied, starting with a separation of 2.3 Å for the lowest concentrations, but got gradually smaller as the hydrogen concentration grew (down to 1.9 Å for the largest considered concentration), due to the steadily increasing volume requirement per hydrogen atom; see results in Sec. III. The volume of the supercell was thereafter varied in a series of steps and, for each case, the coordinates were allowed to relax while the supercell lattice vectors were kept fixed and cubic. The pressure was then calculated from the final equilibrium structure and, by fitting the resulting volume vs pressure curve, the volume corresponding to zero external

pressure could be determined. This procedure was performed for multiple concentrations of hydrogen and, from the resulting configurations, the volume expansion could be calculated. This process was also repeated with the added constraint that the two in-plane supercell lattice vectors were kept fixed throughout the concentration interval to mimic the clamping behavior expected to be present in the measured film, but, in this case, the volumes that corresponded to a zero out-of-plane stress were the ones extracted. The in-plane stress of each clamped system was also extracted and used to determine the components of the dipole force tensor.

Without loss of generality, the diagonal components of the dipole tensor can be considered to be of the form $\text{diag}(\mathbf{P}^\Gamma) = \{B^\Gamma, B^\Gamma, A^\Gamma\}$, with B corresponding to the in-plane components, while A corresponds to the out-of-plane component and the superscript signifies whether the system is clamped or not ($\Gamma = \{\text{clamped, isotropic}\} \equiv \{\text{cl, iso}\}$). Under this assumption, the symmetries associated with both the isotropic and clamped boundary conditions are taken into account. Following the approach outlined in Ref. [36], the isotropic expansion is of the form

$$\left(\frac{\Delta V}{V_0}\right)^{\text{iso}} = \frac{c}{\Omega} (S_{11} + 2S_{12}) \text{Tr}(\mathbf{P}^{\text{iso}}), \quad (3)$$

in which S_{ij} corresponds to the compliance constants, related to the elastic constants C_{ij} via its inverse $\mathbf{S} = \mathbf{C}^{-1}$. For the clamped case,

$$\left(\frac{\Delta V}{V_0}\right)^{\text{cl}} = \frac{c}{\Omega} \frac{(S_{11} - S_{12})(S_{11} + 2S_{12})}{S_{11} + S_{12}} A^{\text{cl}}, \quad (4)$$

the volume expansion is directly proportional to the out-of-plane component A . To obtain B , and thus the complete dipole tensor, one also needs to consider the in-plane stress ($\sigma_{xx} = \sigma_{yy} \equiv \sigma$), which can be expressed as

$$\sigma = -\frac{c}{\Omega} \left(B^{\text{cl}} + \frac{S_{12}}{S_{11} + S_{12}} A^{\text{cl}} \right). \quad (5)$$

Via the elastic response associated with an isotropic free and clamped expansion, the relative thickness expansions can be related to one another according to

$$\left(\frac{\Delta d}{d_0}\right)^{\text{cl}} = \left(1 - \frac{2S_{12}}{S_{11} + S_{12}}\right) \left(\frac{\Delta d}{d_0}\right)^{\text{iso}}, \quad (6)$$

which makes it possible to determine the isotropic volume expansion as long as the elastic compliance constants and the clamped thickness expansion are known.

The elastic H-H interaction energy u can be expressed in terms of the trace of the dipole tensor, as derived by Alefeld in Ref. [37]. Rewriting it in terms of the compliance constants one obtains

$$u^\Gamma = -\frac{4}{9} \frac{(S_{11} + 2S_{12})^2}{S_{11} + S_{12}} \frac{\text{Tr}(\mathbf{P}^\Gamma)^2}{\Omega}. \quad (7)$$

III. RESULTS

Prior to the neutron measurements, the sample was measured with x-ray diffraction, using both symmetric and grazing incidence configurations, neither of which revealed any evidence of crystallinity, as shown in the Supplemental

Material [38], Fig. S1. The room temperature resistivity was measured to be $152.3 \mu\Omega \text{ cm}$, and exhibited a negative temperature coefficient $\alpha = -1.6 \times 10^{-4} \text{ K}^{-1}$, both of which are typical for metallic glasses [39]. We conclude therefore that the sample is amorphous.

Neutron reflectivity patterns of the film taken at selected deuterium pressures are shown in Fig. 1(a). As can be seen in the figure, the deuterium causes systematic changes in the amplitude of the fringes, indicating that the difference between the scattering length density of the substrate, vanadium-zirconium, and palladium layers is decreasing. Also clearly visible in the pattern is a shift towards lower wave vector values, indicative of a thickness expansion.

The patterns were fitted with a slab model as described in Sec. II and the fitted scattering length density profiles are shown in Fig. 1(b). Three features can immediately be highlighted: first, the scattering length density profiles systematically shift towards higher values as the external deuterium pressure goes up. This is a clear sign that the deuterium concentration is increasing. Second, the deuterium-induced thickness expansion can be directly seen by the shift of the right side of the profiles, which marks the surface of the film. Finally, two regions, one close to the substrate and the other at the interface between the glass and the palladium capping layer, marked (II) and (IV) in the figure, were found to contain less deuterium than the interior layer. These partially depleted regions have also been found in superlattices of Fe/V and Mo/V [40] and are due to charge transfer and/or interdiffusion between the metallic glass and the substrate or the cap layer. The width of these two layers were kept constant in the slab model; only the changes in thickness of region (III) were used for determining the volume expansion coefficient.

After the first loading cycle at 423 K, the sample was allowed to partially desorb in ultrahigh vacuum for 6 h before the entire procedure was repeated for the two temperatures that are shown in Fig. 2. But, given the temperature and time constraints of the measurements, it was not possible to entirely empty the sample before starting a new cycle, on account of the strong negative enthalpy of solution for hydrogen in the metal. The structure was found to be completely intact after each isotherm, as evidenced by nearly identical reflectivity patterns taken at $c \approx 0.4 \text{ H/M}$, as shown in the Supplemental Material [38], Fig. S2. The fact that the interference oscillations are still present and are virtually identical after several partial loading cycles strongly suggests that no in-plane expansion is taking place. If such an expansion had occurred, one would expect cracking and/or peeling of the film as it extrudes and retracts past the substrate during absorption and desorption, which consequently would alter the reflectivity patterns greatly.

Furthermore, the expansion curves at different temperatures following the same trend irrespective of the temperature is further evidence of the reversible nature of the expansion. After the neutron measurements, the sample was measured once again with x-ray diffraction and still no evidence was found of crystallinity and/or shattering; see Fig. S1 in the Supplemental Material [38]. The absence of in-plane expansion is also found for hydrogen in epitaxial films of Nb(001)/Al₂O₃ (Refs. [41,42]) and superlattices of Fe/V(001) grown on MgO(001) (Ref. [43]), where it was

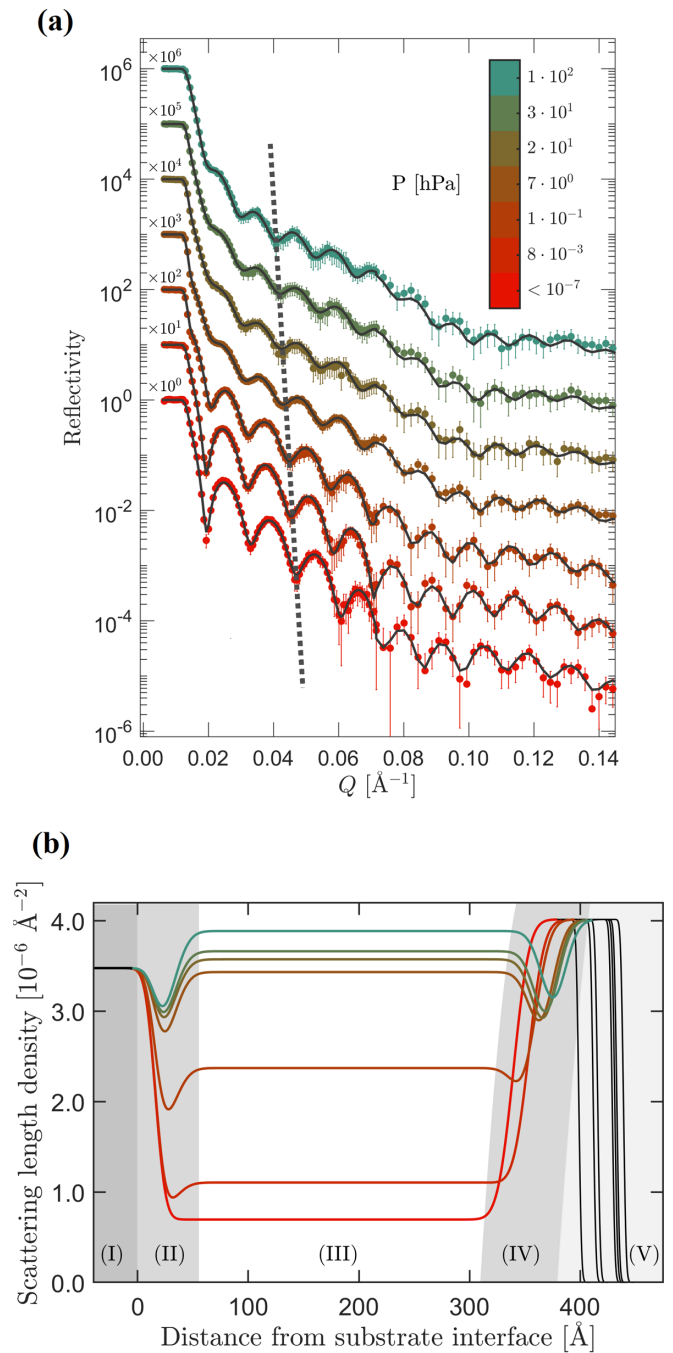


FIG. 1. (a) Neutron reflectivity patterns of a thin film of $V_{80}Zr_{20}$, measured at stepwise increasing D_2 pressures. The reflectivity patterns are on an absolute scale, scaled by the number indicated for clarity. The black solid line is a fit to a slab model using GENX and the dashed line illustrates the gradual contraction of the fringes. (b) Scattering length density profiles determined from the reflectivity patterns. The color coding represents the same selection of pressures as in Fig. 1(a). The substrate is indicated by (I), while (II) and (IV) are denoting the partial depletion regions, (III) is the sample layer, and (V) is the palladium surface layer

thought that the epitaxial nature of the growth improved the adhesion to the substrate. Our results suggest that epitaxy does not appear to be a necessary requirement for the clamping of thin films, which has also been seen in other clamped thin

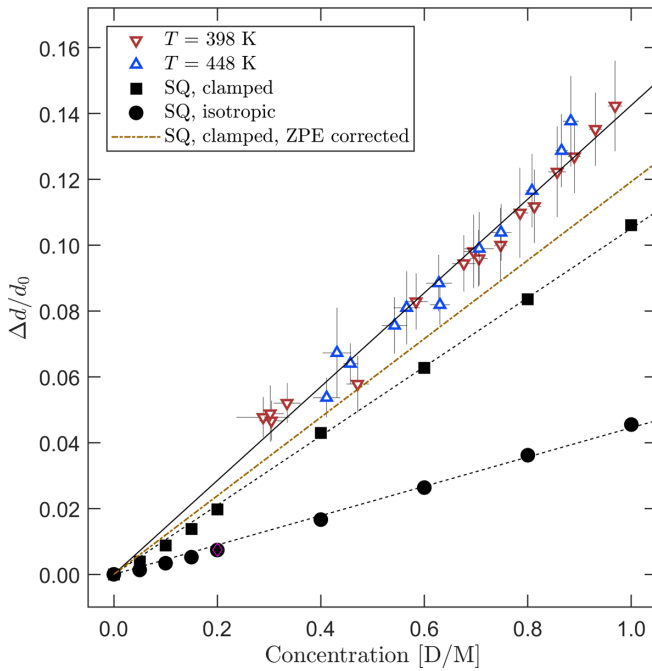


FIG. 2. Relative changes in thickness of the film as a function of deuterium concentration. A linear relationship is found with a slope of 0.143(3) that is independent of temperature. Also shown in the figure is the isotropic and clamped thickness expansion (black circles and squares, respectively) obtained from *ab initio* stochastic quenching (SQ) calculations. The orange dash-dotted line represents the expansion if the zero-point energy (ZPE) of deuterium is taken into account.

amorphous films [44–46]. Given that the x-ray and neutron data are consistent with no plastic deformation (including cracking, peeling, void formation, inclusions, etc.) along with the film adhesion to the substrate, we conjecture that our film is clamped. This could be verified via in-plane stress measurements during hydrogen loading to see whether the stress scales as theoretically predicted in Fig. 4.

The deuterium-induced thickness expansion of the metallic glass is plotted in Fig. 2 as a function of the deuterium concentration in the middle layer. A linear relationship between the thickness changes and the concentration is found with a slope value of $k_{\text{exp}}^{\text{cl}} = 0.143(3)$, which is remarkable considering the fact that this expansion occurs in only one direction. Furthermore, since presumably no, or negligibly small, in-plane expansion occurred, the total relative change in volume also corresponds to the relative thickness expansion, i.e., $(\Delta V/V_0)^{\text{cl}} = (\Delta d/d_0)^{\text{cl}}$. Comparing this to the volume expansion coefficient of bulk zirconium and vanadium with hydrogen occupying tetrahedral sites, we find the volume expansion of clamped amorphous $V_{80}Zr_{20}$ to be larger than that of zirconium, with an expansion coefficient of 0.115 (Ref. [47]), yet lower than that of vanadium, with a value of 0.187 (average of the values in Table 1 of Ref. [36]). Another notable feature is that the linear relationship does not change with respect to temperature, which indicates that the deuterium has not phase separated during the measured temperature and pressure intervals.

To gain deeper insight into the nature of the expansion, we carried out computational simulations in which hydrogen was introduced to the stochastically quenched $V_{80}Zr_{20}$ structure following the procedure outlined in Sec. II and let to either expand freely in all three dimensions (isotropic case) or under the constraint of no in-plane expansion (clamped case). The results are shown in Fig. 2 as black circles (isotropic expansion) and black squares (clamped expansion). Both exhibit, to a first order approximation, a linear coefficient of thickness expansion, each with a slope value of 0.045(1) and 0.105(2). Comparing instead the total volume expansions, each with a respective slope of $k_{\text{SQ}}^{\text{iso}} = 0.139(4)$ and $k_{\text{SQ}}^{\text{cl}} = 0.105(2)$, we notice that the total expanded volume is not conserved, but rather dependent on the elastic boundary conditions. The coefficient of the isotropic volume expansion is surprisingly close to the one found for the clamped experimental slope. However, this is most likely only a coincidence, since, if this would be the case, the Poisson ratio of amorphous $V_{80}Zr_{20}$ has to be equal to 0.5 in order to be consistent with the elastic theory of solids, a value which in itself is very unlikely. What is more probable is for the discrepancy between the experimental and clamped theoretical slopes to originate from inadequacies in the PBE GGA functionals, as has also been noticed in other first-principles studies [48–51], or that other phenomena could be at play, such as complex vacancy defect formations [52].

Additionally, one consequence of the Born-Oppenheimer approximation in DFT is that the zero-point motion of the atoms are not naturally taken into account. For metallic systems, this effect is small, but for hydrogen and deuterium with their low mass, the zero-point energy (ZPE) could be significant enough to cause additional local strain and thus further expand the metal. We have estimated the significance of the ZPE of deuterium on the volume expansion and the procedure is summarized in the Appendix. In Fig. 2 we illustrate the magnitude of this correction as applied on the clamped expansion, and we obtain about a 14% improvement, which is still not enough to describe the discrepancy between theory and experiments. However, we show here that this effect cannot be neglected and should be kept in mind when studying the effects of hydrogen in metals.

Another way to visualize the volume expansion is to examine the volume change per hydrogen atom, Δv , which we determine from the experimental slope to have an average value of $2.31(6) \text{ \AA}^3/\text{D atom}$, which is within the interval of hydrogen volumes that Westlake determined for crystalline vanadium, zirconium, and the intermetallic V_2Zr (Ref. [14]). On the other hand, Δv in our theoretical calculations can be directly determined by assessing the total change in volume of the considered hydrogen-loaded supercells. The results are shown in Fig. 3. Interestingly, the volume that hydrogen displaces in the amorphous metal varies significantly with concentration and, moreover, depending on whether the structure is clamped or not, that volume requirement is also distinctly different. The Δv of the isotropic case approaches, coincidentally, the experimental value at higher concentrations, while Δv from the clamped expansion essentially saturates at around hydrogen concentrations of about 0.4 H/M. Furthermore, the occupied hydrogen volume in both cases drops as low as $1.2 \text{ \AA}^3/\text{D atom}$ in concentrations of around 0.05 H/M. This shows that the volume that hydrogen

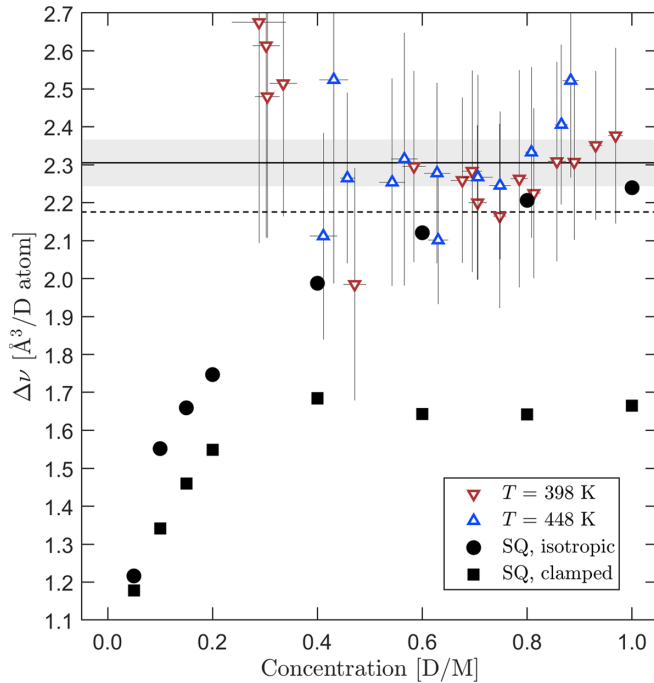


FIG. 3. Volume one deuterium atom requires ($\Delta\nu$) as a function of deuterium concentration. The black solid line corresponds to the estimated average volume change from the experimental slope, calculated via the procedure outlined in Ref. [10], and the gray area represents the width of its standard deviation. The dashed black line is determined via the slope of the theoretical isotropic volume expansion curve following the same approach. The black squares and circles are explicit theoretical calculations of $\Delta\nu$ from the change in volume of the supercells.

requires in metallic glass varies with concentration and is highly dependent on the elastic boundary conditions of the system.

Due to the constraint of no in-plane expansion for the clamped theoretical system, a buildup of in-plane stress had to occur to expand the system in the out-of-plane direction. The calculated average in-plane stress is shown in Fig. 4. The nonlinear increase of the stress, as illustrated by a second-order polynomial fit, reflects that it is not sufficient to only consider linear responses for arbitrarily large concentrations of hydrogen.

IV. DISCUSSION

As a caveat, due to the additional expansion in terms of the zero-point energy correction, the theoretical volume change per hydrogen, as well as the in-plane stress, the dipole tensor components, and the H-H interaction should also be larger in magnitude than shown here, but, for the sake of consistency, we opted to only display the results from DFT here as lower bounds on all resulting quantities.

The volume change per hydrogen atom, $\Delta\nu$, represents the average volume that hydrogen displaces in order to occupy a site location. Interestingly, but coincidental as mentioned before, both experiment and theory, in particular the isotropic case, predict similar deuterium volumes to be present at higher concentrations, but for lower concentrations our

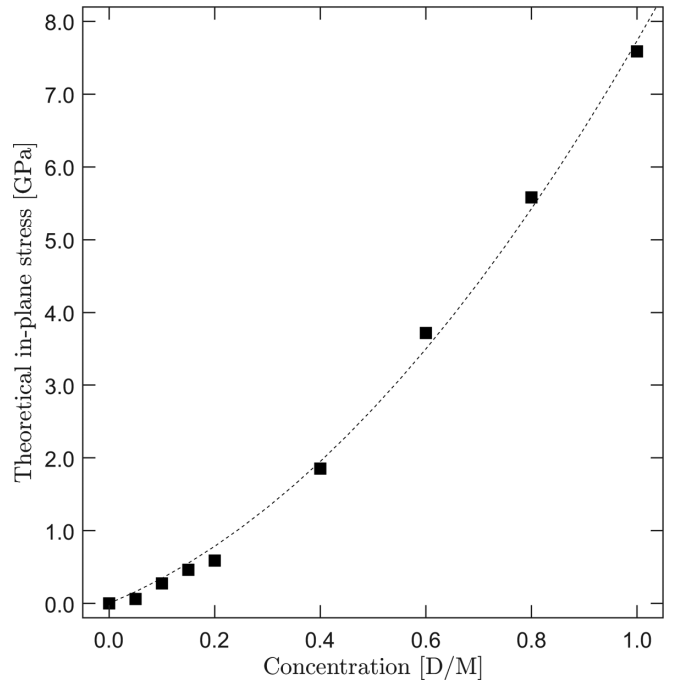


FIG. 4. Black squares correspond to the calculated in-plane stress of the clamped metal-hydrogen system, whereas the dashed line is a second-order polynomial fit. The gradual nonlinear increase suggests that higher order terms are relevant when dealing with hydrogen-induced stress in metallic glasses.

calculations instead show that the volume requirement decreases. This trend has also been observed in other metallic glasses [15,16,53], which further demonstrates that the concept of constant site volumes and H-H distances in crystalline hydrides, proposed by Westlake, might not be directly transferable to metallic glasses. Instead, as a consequence of the distribution of local atomic environments, a broad range of available sites and site volumes, which are successively filled until a mean site volume occupancy has been reached, allows for a greater variety of possible hydrogen volumes. The low concentration regime where these effects are the most prominent was inaccessible in our experiment, in part due to the exceedingly low pressure requirements for those concentrations.

As mentioned in the Introduction, the hydrogen-induced volume changes carry significant information about the elastic distortions and the strain fields in the material, the central quantity of which is the dipole force tensor. The out-of-plane component A^{cl} can be extracted via the slope of the relative change in thickness, as long as the elastic (or compliance) constants of the metallic glass are known. To our knowledge, the elastic constants have not been determined for amorphous $V_x\text{Zr}_{1-x}$; therefore, we have calculated them from first principles. The material was assumed to be isotropic and the elastic constants were determined as described in Sec. II and are summarized in Table I. With these constants in hand, we can test the validity of the elastic theory of solids for amorphous systems by transforming the isotropic thickness expansion to a clamped one via Eq. (6), in which we find that the converted and explicit slopes only differ by about 0.8%.

TABLE I. The left side of the table shows the elastic and compliance constants calculated from the stochastically quenched structure in units of GPa and TPa⁻¹, respectively. The right side of the table shows the engineering constants (in the units of GPa, except for μ , which is dimensionless), bulk modulus (B), Young's modulus (Y), shear modulus (G), and Poisson's ratio (μ), assuming the solid is isotropic. The error bars arise from the standard deviation of the isotropic averaging.

C_{11}	C_{12}	C_{44}	S_{11}	S_{12}	S_{44}	B	Y	G	μ
178(3)	122(1)	28(2)	12.9(4)	-5.3(4)	36(2)	141(1)	78(5)	28(1)	0.408(5)

This demonstrates that elasticity theory, in combination with the incorporation of hydrogen into stochastically quenched structures, is internally consistent in evaluating the hydrogen-induced changes in metallic glasses.

Therefore, using these constants, we calculate from the experimental slope via Eq. (4) the clamped out-of-plane dipole component and find $A^{\text{cl}} = 2.55(5)$ eV. This value is very similar to a composition-weighted sum of the out-of-plane components found in vanadium [36] and zirconium [49], suggesting the dipole tensor in a metallic glass can to a large extent be estimated by a superposition of its constituents' dipole tensors. However, to validate this hypothesis, measurements of the dipole tensors of other compositions need to be conducted in order to determine whether the dipole tensor of metallic glasses truly exhibit such a close connection to their elemental composition.

To determine the in-plane component B^{cl} one has to measure the clamped in-plane stress, which was not possible with the *in situ* neutron chamber. The in-plane stress however is accessible in the *ab initio* calculations for the clamped system. As can be observed in Fig. 4, second-order terms of the stress become increasingly relevant already at concentrations of around 0.2 H/M. We will therefore separate the analysis into two categories: one that considers only the concentration regions where the linear term is still applicable, i.e., below 0.2 H/M, while the other assumes that the dipole components are implicit functions of hydrogen concentrations, $A^{\text{T}}(c)$ and $B^{\text{T}}(c)$, as also suggested by Berry and Pritchett [54] to be possible in disordered solids. In the first case, we use the slope (up to 0.2 H/M) of the relative thickness expansion and the linear term from the fit of the in-plane stress from Fig. 4 and calculate A^{cl} and B^{cl} via a combination of Eq. (4) and Eq. (5) for the clamped system, while the trace of the dipole tensor is determined via Eq. (3) for the isotropic case. All results are summarized in Table II.

Implementing the same equations for the variable dipole case, in which the whole concentration range is taken into account, one obtains the results shown in Fig. 5. The striking similarity of these results to the Δv in Fig. 3 highlights how closely related the dipole forces and the hydrogen-induced strain are. Furthermore, converting the trace of the concentration dependent dipole tensor derived from the clamped thickness expansion and in-plane stress to Δv [via $\Delta v = (S_{11} + 2S_{12})\text{Tr}(\mathbf{P})$, Ref. [10]] reveals that this quantity is identical within 1.5% with the explicitly calculated Δv , which validates the assumption of the dipole tensor being concentration dependent. Another notable feature is the striking similarity between the clamped and isotropic dipole traces, both in the tabulated values (Table II) and in its variable form (Fig. 5), which suggests that the average of the dipole forces

conform to approximately the same value, irrespective of the symmetries of the system.

With the transformation in Eq. (6) now verified, we propose that it is possible to determine both the clamped and isotropic volume expansions from only performing studies on a clamped system or a freely expanded one, if the elastic constants are known. We can therefore convert the clamped experimental expansion to an isotropic one by using the calculated elastic constants and Eq. (6), in which we find a relative volume expansion slope of $k_{\text{exp}}^{\text{iso}} = 0.188(4)$, which is exceedingly close to the expansion rate of crystalline bulk vanadium [36]. From this, we estimate the trace of the isotropic dipole tensor to be at a value of around 2.67(6) eV, which also is remarkably close to the values of vanadium [36].

The physical quantity that governs the elastic attraction between hydrogen atoms, and which is in part responsible for hydrogen phase separation in metals, is the elastic H-H interaction. By using the values of the dipole tensor, as well as the compliance constants, we estimate the H-H interaction energy via Eq. (7) for both the theoretical systems and the estimated experimental isotropic expansion. The theoretical values corresponding to the constant dipole terms, i.e., below 0.2 H/M, and the experimentally estimated value are displayed in Table II. As for the theoretical results, we observe here a striking similarity between the two values, which suggests that the elastic distortions in the metallic system mediate the interaction independent of the elastic boundary conditions of the material. For the case when the dipole tensor components vary with hydrogen concentration, shown in Fig. 5, the attractive strength of the H-H interaction gets stronger with increasing concentration. Again we observe, due to the similar trace of the clamped and isotropic tensor, that the H-H

TABLE II. Expansion coefficients extracted from the slopes of the thickness change vs concentration curves. From the experimental and theoretical slopes, the components and trace of the dipole tensor and the H-H interaction energy are all in units of eV except k , which is dimensionless. Values denoted with † are estimated using the transformation according to Eq. (6) and values displayed with * are only evaluated up to 0.2 H/M.

	Experiment		Theory	
	Clamped	Isotropic	Clamped	Isotropic
k	0.143(3)	0.188†(4)	0.105(1)	0.139(4)
A	2.55(5)		1.64*(3)	
B			1.42*(2)	
$\text{Tr}(\mathbf{P})/3$		2.67†(6)	1.50*(2)	1.48*(4)
u		-0.209†(9)	-0.067*(2)	-0.066*(3)

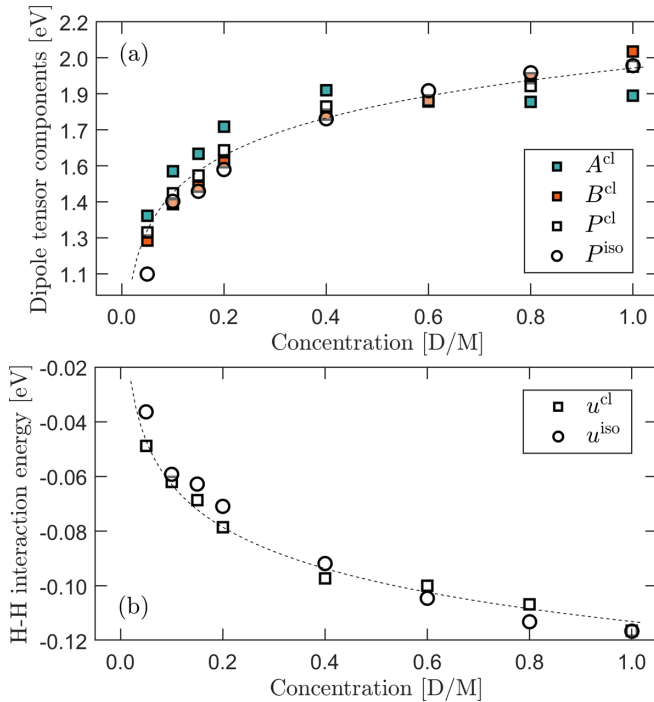


FIG. 5. (a) Calculated dipole tensor components as a function of hydrogen concentration, as determined via Eq. (4) and Eq. (5) for the clamped system and Eq. (3) for the isotropic one. (b) Calculated elastic H-H interaction energy as a function of hydrogen concentration, determined via Eq. (7). For both graphs, the dashed lines are guides for the eye.

interaction also practically overlaps, irregardless of the global boundaries of the system, which further demonstrates that a long-range order and other symmetries present in crystals are not necessary requirements for the existence of the nonlocal elastic H-H interaction. Furthermore, as a consequence of the concentration-dependent strength of the interaction, the conditions regarding a possible hydrogen phase decomposition in amorphous materials, introduced by Griessen [8], could also change and evolve with the amount of hydrogen in the metal.

V. CONCLUSIONS

Neutron reflectometry is found to be exceedingly useful in determining the deuterium-induced thickness expansion for thin metallic glasses. The metal, subject to several absorption and partial desorption cycles, is free of any apparent structural degradation, even though the volume expanded by more than 14% in one direction. Under the assumption that the experimentally measured sample was fully clamped and that the theoretical elastic constants are reasonable, we estimate an out-of-plane dipole tensor component remarkably similar to a composition-weighted sum of the ones found in crystalline vanadium and zirconium, suggesting that the dipole tensors related to metallic glass can to a large extent be described by a superposition of its constituents' dipole tensors.

Density functional theory calculations reveal that the elastic theory of solids is applicable for disordered amorphous systems and is able to self-consistently predict the free and biaxially constrained expansions of the system. The discrep-

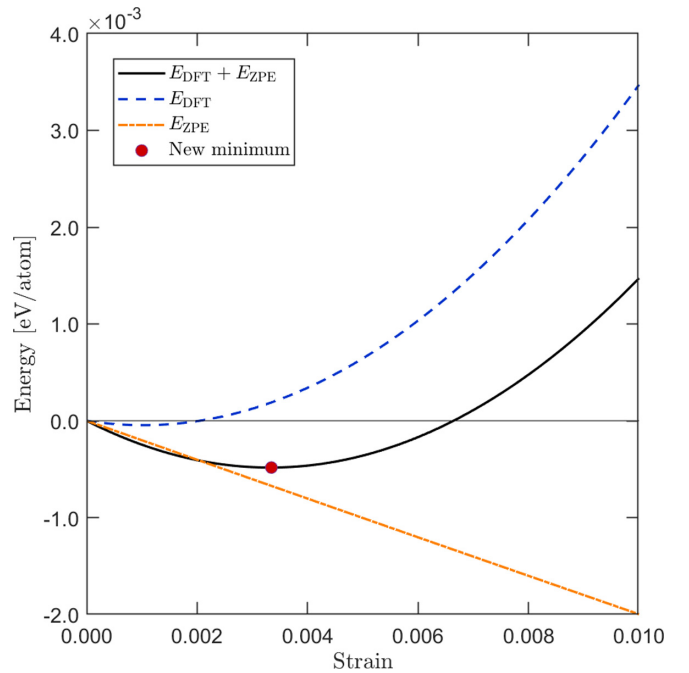


FIG. 6. Shift in energy minimum if the zero-point energy (ZPE) of deuterium is taken into account. The functions are normalized to zero for illustrational purposes.

any between the clamped theoretical volume expansion and the observed experimental change in volume stem most likely from inadequacies of the GGA functionals in evaluating the hydrogen-induced forces, and from the fact that the zero-point motion of hydrogen is not taken into account. By calculating the phononic vibrational modes of hydrogen, we show that the zero-point energy will have a non-negligible effect on the expansion and should be considered in studies of hydrogen in metals.

The volume dilations per hydrogen atom are greatly affected by the elastic boundary conditions, while the average dipole tensor component is found to be largely invariant. Assuming that the dipole tensor components vary with hydrogen content, all observed quantities (volume expansions, hydrogen occupation volumes, and average stress) are internally consistent following the formalism of the elastic theory of point defects, suggesting that the distribution of local atomic environments can allow for a systematically varying, but non-trivial, dipole tensor. With a functional form of the dipole force tensor, the magnitude of the attractive H-H interactions increases with hydrogen concentration and is shown to be independent of the global elastic boundary conditions, suggesting that a long-range order and other symmetries present in crystals are not necessary requirements for the mediation of the nonlocal H-H interaction in metallic glasses.

Hence, manifested in the dipole tensor, a conceptual framework emerges for the study of local and global volume changes in metallic glasses.

ACKNOWLEDGMENTS

The authors gratefully acknowledge the Swedish Research Council (VR - Vetenskapsrådet) Grant No. 2018-05200 for

funding the work and the Swedish Energy Agency Grant No. 2020-005212. G.K.P. also acknowledges the Carl-Tryggers foundation Grants No. CTS 17:350 and No. CTS 19:272 for financial support. The computations were enabled by resources provided by the Swedish National Infrastructure for Computing (SNIC), partially funded by the Swedish Research Council through Grant Agreement No. 2018-05973. The SuperADAM project acknowledges the Swedish Research Council for support.

APPENDIX

The zero-point energy of deuterium is determined via phonon calculations, performed using the PHONOPY package

[55], in which a series of expanded supercells containing 0.5 H/M were used to determine the vibrational energies of the material. The isotope mass was corrected for by a factor of $2^{-1/2}$, corresponding to the inverse square root proportionality between mass and phonon energies. By integrating the phonon density of states in a frequency region corresponding to the hydrogen vibrational modes, the zero-point energy as a function of strain could be determined and added to the ground state energy of DFT as a function of strain. The resulting combined energy curve, shown in Fig. 6, exhibits a minimum about 0.33% above the determined optimal relaxed thickness, which results in an isotropic thickness expansion of $k_{\text{SQ}}^{\text{iso}} = 0.060$ and, via the transformation of Eq. (6), a clamped thickness expansion of $k_{\text{SQ}}^{\text{cl}} = 0.119$. The thus corrected slope is shown in Fig. 2.

-
- [1] A. Borgschulte, *Front. Energy Res.* **4**, 11 (2016).
- [2] L. Bannenberg, H. Schreuders, and B. Dam, *Adv. Funct. Mater.* **31**, 2170110 (2021).
- [3] H. T. Lu, W. Li, E. S. Miandoab, S. Kanehashi, and G. Hu, *Front. Chem. Sci. Eng.* **15**, 464 (2021).
- [4] A. El Kharbachi, O. Zavorotynska, M. Latroche, F. Cuevas, V. Yartys, and M. Fichtner, *J. Alloys Compd.* **817**, 153261 (2020).
- [5] M. Nagumo, *Fundamentals of Hydrogen Embrittlement* (Springer, Berlin, 2016).
- [6] H. Wagner and H. Horner, *Adv. Phys.* **23**, 587 (1974).
- [7] P. M. Richards, *Phys. Rev. B* **30**, 5183 (1984).
- [8] R. Griessen, *Phys. Rev. B* **27**, 7575 (1983).
- [9] G. Leibfried and N. Breuer, *Point Defects in Metals I, Springer Tracts in Modern Physics*, Vol. 81 (Springer, Berlin, 1978).
- [10] H. Peisl, in *Hydrogen in Metals I*, edited by G. Alefeld and J. Völkl, Topics in Applied Physics, Vol. 28 (Springer, Berlin, 1978), p. 53.
- [11] A. C. Switendick, Report No. SAND-79-0493C 10.2172/6694106, 1978 (unpublished).
- [12] A. C. Switendick, *Z. Phys. Chem.* **117**, 89 (1979).
- [13] D. Westlake, *J. Less-Common Met.* **91**, 1 (1983).
- [14] D. Westlake, *J. Less-Common Met.* **90**, 251 (1983).
- [15] H. Mizubayashi, M. Shibasaki, and S. Murayama, *Acta Mater.* **47**, 3331 (1999).
- [16] U. Stolz, U. Nagorny, and R. Kirchheim, *Scr. Metall.* **18**, 347 (1984).
- [17] S. Hong and C. L. Fu, *Phys. Rev. B* **66**, 094109 (2002).
- [18] L. Q. Shi and S. L. Xu, *J. Vac. Sci. Technol. A* **24**, 190 (2006).
- [19] F. Trequattrini, F. Cordero, G. Cannelli, R. Cantelli, A. Coda, and A. Gallitognotta, *J. Alloys Compd.* **438**, 190 (2007).
- [20] A. Borgschulte, J. Terreni, E. Billeter, L. Daemen, Y. Cheng, A. Pandey, Z. Łodziana, R. J. Hemley, and A. J. Ramirez-Cuesta, *Proc. Natl. Acad. Sci. USA* **117**, 4021 (2020).
- [21] R. Hempelmann, D. Richter, O. Hartmann, E. Karlsson, and R. Wäppling, *J. Less-Common Met.* **104**, 209 (1984).
- [22] E. Holmström, N. Bock, T. Peery, E. Chisolm, R. Lizárraga, G. DeLorenzi-Venneri, and D. Wallace, *Phys. Rev. B* **82**, 024203 (2010).
- [23] M. Kaplan, J. Bylin, P. Malinovskis, R. H. Scheicher, and G. K. Pálsson, *Materialia* **24**, 101496 (2022).
- [24] F. D. Manchester, A. San-Martin, and J. M. Pitre, *J. Phase Equilib.* **15**, 62 (1994).
- [25] A. Vorobiev, A. Devishvilli, G. Pálsson, H. Rundlöf, N. Johansson, A. Olsson, A. Dennison, M. Wolff, B. Giroud, O. Aguetaz, and B. Hjörvarsson, *Neutron News* **26**, 25 (2015).
- [26] M. Björck and G. Andersson, *J. Appl. Crystallogr.* **40**, 1174 (2007).
- [27] M. Björck, *J. Appl. Crystallogr.* **44**, 1198 (2011).
- [28] V. F. Sears, *Neutron News* **3**, 26 (1992).
- [29] W. Kohn and L. J. Sham, *Phys. Rev.* **140**, A1133 (1965).
- [30] P. Hohenberg and W. Kohn, *Phys. Rev.* **136**, B864 (1964).
- [31] G. Kresse and J. Furthmüller, *Phys. Rev. B* **54**, 11169 (1996).
- [32] G. Kresse and J. Furthmüller, *Comput. Mater. Sci.* **6**, 15 (1996).
- [33] G. Kresse and J. Hafner, *Phys. Rev. B* **47**, 558 (1993).
- [34] J. P. Perdew, K. Burke, and M. Ernzerhof, *Phys. Rev. Lett.* **77**, 3865 (1996).
- [35] M. Methfessel and A. T. Paxton, *Phys. Rev. B* **40**, 3616 (1989).
- [36] G. K. Pálsson, M. Wälde, M. Amft, Y. Wu, M. Ahlberg, M. Wolff, A. Pundt, and B. Hjörvarsson, *Phys. Rev. B* **85**, 195407 (2012).
- [37] G. Alefeld, *Berichte der Bunsengesellschaft für physikalische Chemie* **76**, 746 (1972).
- [38] See Supplemental Material at <http://link.aps.org/supplemental/10.1103/PhysRevB.106.104110> for the x-ray diffraction and reflectivity patterns depicting the reversible nature of the expansion.
- [39] U. Mizutani, *Prog. Mater. Sci.* **28**, 97 (1983).
- [40] B. Hjörvarsson, G. Andersson, and E. Karlsson, *J. Alloys Compd.* **253-254**, 51 (1997).
- [41] P. Miceli, H. Zabel, J. Dura, and C. Flynn, *J. Mater. Res.* **6**, 964 (1991).
- [42] G. Song, A. Remhof, K. Theis-Bröhl, and H. Zabel, *Phys. Rev. Lett.* **79**, 5062 (1997).
- [43] G. K. Pálsson, A. R. Rennie, and B. Hjörvarsson, *Phys. Rev. B* **78**, 104118 (2008).
- [44] I. Fernández-Martínez, J. L. Costa-Krämer, and F. Briones, *J. Appl. Phys.* **103**, 113902 (2008).
- [45] V. Lyahovitskaya, Y. Feldman, I. Zon, A. Yoffe, and A. I. Frenkel, *J. Mater. Res.* **27**, 2819 (2012).

- [46] V. Lyahovitskaya, Y. Feldman, I. Zon, E. Wachtel, K. Gartsman, A. K. Tagantsev, and I. Lubomirsky, *Phys. Rev. B* **71**, 094205 (2005).
- [47] S. MacEwen, C. Coleman, C. Ells, and J. Faber, *Acta Metall.* **33**, 753 (1985).
- [48] C. Domain, R. Besson, and A. Legris, *Acta Mater.* **50**, 3513 (2002).
- [49] R. Nazarov, J. S. Majevadia, M. Patel, M. R. Wenman, D. S. Balint, J. Neugebauer, and A. P. Sutton, *Phys. Rev. B* **94**, 241112(R) (2016).
- [50] C. Varvenne and E. Clouet, *Phys. Rev. B* **96**, 224103 (2017).
- [51] K. A. Moltved and K. P. Kepp, *J. Phys. Chem. A* **123**, 2888 (2019).
- [52] Y. Fukai and H. Sugimoto, *J. Phys.: Condens. Matter* **19**, 436201 (2007).
- [53] D. Menzel, A. Niklas, and U. Köster, *J. Mater. Sci. Eng. A* **133**, 312 (1991).
- [54] B. S. Berry and W. C. Pritchett, *Mechanical Relaxation Behavior of Hydrogenated Metallic Glasses*, *NATO Advanced Studies Institute, Series B: Physics* (Plenum, New York, 1986), p. 215.
- [55] A. Togo and I. Tanaka, *Scr. Mater.* **108**, 1 (2015).